

# Depth migration velocity model building with wave equation imaging

Joe Higginbotham<sup>1</sup>, Morgan Brown<sup>1\*</sup> and Cosmin Maccesanu<sup>1</sup>

---

## Abstract

In spite of impressive advances in the application of wave equation imaging technology to generate images of complex structures, ray-based tools are generally used for the equally important step of velocity determination. Closing the experimental loop, by using the same wave equation imaging algorithm to measure velocity and to obtain a final image, is more than just philosophically pleasing. In strata exhibiting complex velocity structure, wave equation migration algorithms may be the only tools able to image some reflectors, so it stands to reason in such cases that only a wave equation velocity update can reliably measure velocity errors near these reflectors. In this article, we present a wave equation velocity update scheme, similar to depth focusing analysis, utilizing the time-shift imaging condition. We demonstrate the robustness of this approach under salt and in a land fault shadow example with limited acquisition effort. A common criticism levied against wave equation migration is the difficulty in efficiently obtaining 3D angle gathers (incidence, azimuth, and dip angle). We also present an efficient Fourier-domain angle decomposition technology for wave equation migration and demonstrate efficacy on synthetic and field data examples.

---

## Introduction

It is widely understood that in regions with significant geological complexity, velocity analysis using depth migration is superior to methods which operate on prestack time echo data. Migration in general, and prestack depth migration (PreSDM) in particular, simplify prestack data by correcting recorded waves for the effects of offset, reflector dip, and propagation in a heterogeneous medium. The most common migration velocity analysis techniques attempt to flatten Kirchhoff PreSDM common-offset depth migration gathers by measuring depth error as a function of offset and perturbing the migration velocity accordingly, either by vertical update or tomographic inversion.

The mid-to-late 1990s saw 3D Kirchhoff PreSDM and related velocity update schemes rise to prominence, placing depth focusing analysis techniques (Faye and Jeannot, 1986; MacKay and Abma, 1992; Audebert and Diet, 1992), which rely on more computationally expensive wave equation migration (WEM), into a state of dormancy. However, the rise of commodity high-performance computing in the first decade of the new millennium renewed attention on WEM depth focusing analysis and other WEM-based velocity update techniques like waveform inversion (e.g., Vigh and Starr, 2008), one-way WEM inversion (Sava, 2004), and hybrid methods (e.g., Fliedner and Bevc, 2008; Wang et al., 2008). No single WEM velocity update method has emerged as clearly superior to the others.

We argue, and illustrate with examples, that depth focusing analysis is a robust option for velocity estimation, not

just in the deepwater Gulf of Mexico subsalt, but also in difficult land examples where topography, irregular sampling, and noise prove too challenging for conventional migration velocity analysis methodologies.

Claerbout (1985) described the one-way wave equation downward continuation process for CMP gathers as ‘survey sinking’. When the migration velocity is correct, all the energy on a downward continued gather is focused at zero time and zero offset when the imaging depth equals the event depth. This forms the basis of Claerbout’s prestack imaging condition for WEM. By measuring mis-focusing either in time, ‘subsurface offset’, or both, measures of velocity error can be developed. WEM subsurface offset gathers have been converted to angle gathers by slant-stacking (Prucha et al., 1999; Rickett and Sava, 2002; Sava and Fomel, 2003), and used for velocity updates (Clapp, 2001; Sava, 2004). Shen et al. (2003) described a velocity update method which uses mis-focusing in subsurface offset directly. On the other hand, WEM depth focusing analysis measures focusing as a function of time, using the so-called time-shift imaging condition (Sava and Fomel, 2006). The previously published depth focusing analysis techniques are qualitatively similar to the techniques of Shen et al. (2003), in that they measure the depth corresponding to best focusing and invoke mathematical relationships to relate measured depth error to a velocity perturbation. We present a variant on depth focusing analysis similar to that of Higginbotham (1993). Rather than pick the focusing depth, we convert the time-shift parameter directly to a perturbation in RMS velocity and, finally, con-

<sup>1</sup>Wave Imaging Technology, 11777 Katy Freeway #156, Houston, TX77079, USA.

\*Corresponding author, E-mail: morgan@wvmgtk.com

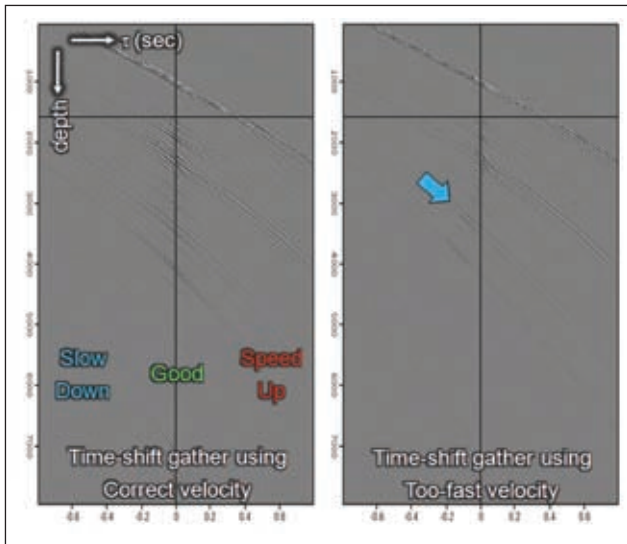


**Figure 1** Left panel shows a time-shift gather obtained by migrating the BP velocity benchmark synthetic data with the true velocity. Events on the time-shift gather are focused about the zero time shift ( $\tau$ ) line. Right panel shows a time-shift gather at the same  $x$  location, obtained by migrating the data with too high a velocity. The arrow points to events which focus best at  $\tau < 0$ , implying that the migration velocity is indeed too fast.

vert to interval velocity using the Dix equation. The velocity perturbations could alternatively be back-projected along traced rays in a reflection tomography scheme. We call our method wave equation migration velocity focusing analysis, or MVFA. The theory underlying MVFA is outlined by Higginbotham et al. (2008).

We found that the accuracy of our MVFA theory could be improved by incorporating reflector dip angle. We also use the dip measurement to form time-shift supergathers by combining time-shift information from adjacent ( $x, y$ ) locations. Thus we needed a means of measuring dip angle directly inside our one-way shot record WEM algorithm. As mentioned above, previous authors have used the space-shift or time-shift imaging condition, coupled with a slant stack, to indirectly compute incidence angle gathers. Biondi and Symes (2003) sketched a general approach to compute 3D angle gathers (incidence and azimuth angles plus, by deduction, dip angle) which requires applying the fairly expensive space-shift imaging condition in  $x$  and  $y$  at every gather location, and then applying a slant stack across the  $x$  and  $y$  lags. We took a strategy similar to Yoon and Marfurt's (2006) more efficient approach for generating 3D angle gathers for reverse-time migration (RTM) to work with our Fourier-domain shot record WEM algorithm. In our method, the imaging condition and angle decomposition are intimately related. In a nutshell, propagation direction vectors of the source and receiver wavefields are computed at all points in an image, allowing us to form fully-sampled angle 'volumes' corresponding to a finite angle range. Higginbotham and Brown (2009) described the implementation of this method.

In addition to providing dip angle information to aid MVFA, our angle decomposition technology represents a

significant advance in the imaging of complex geology. By better understanding illumination both in incidence angle and azimuth angle, we can unravel the effects of deficiencies in acquisition and data pre-processing, as well as use the angle information for either direct velocity update or velocity QC.

## Method

In one-way shot record WEM, the receiver data from a shot record are Fourier transformed in time and then downward continued in depth. A synthetic point source is similarly downward continued to the position of the shot gather's source location. In the conventional (Claerbout, 1985) imaging condition, the image at the current depth, for all  $x$  and  $y$ , is the zero lag coefficient in the cross-correlation between the receiver and source wave fields. By correlating the wavefields at a non-zero spatial lag (Rickett and Sava, 2002), subsurface offset gathers are formed. Similarly, by applying a time shift to the two shot record migration wavefields, time-shift gathers are formed (Sava and Fomel, 2006).

Figure 1 illustrates the effect of migration velocity errors on time-shift gathers. The first step in the MVFA method is to apply a semblance measure to a time-shift gather. The depth axis of the semblance gather is then converted to time, using the migration velocity. Finally, the  $\tau$ -axis of the semblance gather is transformed to a perturbation in RMS velocity,  $\Delta v$ , according to the relation shown in Higginbotham et al. (2008):

$$\frac{\tau'}{t_v} = -1 + \sqrt{1 + \frac{2 \frac{\Delta v(t)}{v(t)} \left(1 - \frac{\Delta v(t)}{2v(t)}\right)}{\left(1 - \frac{\Delta v(t)}{v(t)}\right)^2}} \quad (1)$$

The quantity  $t_v$  in Equation (1) is vertical travel time. To improve accuracy,  $\tau'$  is implemented as a function of dip angle  $\alpha$ :  $\tau' = \tau \cos \alpha$ . The RMS migration velocity is  $v(t)$ . The measured dip angle is also very important if multiple time-shift-gathers are combined to form super-gathers. Equation (1) represents a horizontal stretch of the time-shift axis of a time-converted time-shift gather into units of velocity perturbation,  $\Delta v$ . When the migration velocity is added to the velocity perturbations, the peak energy should indicate the true RMS velocity. In our current implementation, the velocity perturbations are effectively back-projected vertically and the corrected RMS velocity converted to interval velocity with the Dix equation. However, the perturbations could readily be back-projected along non-normal rays and/or input into a tomographic inversion scheme.

To be clear, MVFA is not using a simple traveltime equation to determine velocity on surface data: we convert a time shift measured at depth by WEM into a velocity perturbation. If the time shift is zero, the velocity perturbation is zero. MVFA does not make any hyperbolic assumptions about the

surface data. At the imaging depth, downward continuation has removed propagation effects due to the overburden.

We also present a method to compute the propagation direction of the source and receiver wavefield in shot record migration, enabling us to compute the incidence angle of a reflection, as well as its azimuth and dip angles. By defining angle ‘bins’, we can create these three types of angle gathers at every point (x,y) in the image, for a nominal incremental cost.

Our angle decomposition scheme for wave equation shot record migration is intimately linked to the phase shift plus interpolation (PSPI) method for solving the one-way factorization of the acoustic wave equation (Gazdag and Squazzero, 1984). Yoon and Marfurt (2006) presented a scheme for computing the propagation direction of a wavefield at a given point (x,y,z) using the Poynting vector. Theirs was a space-domain approach. Here we operate in the 2D (k<sub>x</sub>, k<sub>y</sub>) Fourier domain, since our shot record WEM is a PSPI algorithm. We use the representation of the Poynting vectors in the wavenumber domain, P<sub>i</sub>(k<sub>x</sub>, k<sub>y</sub>, k<sub>z</sub>) = k<sub>i</sub> U(k<sub>x</sub>, k<sub>y</sub>, k<sub>z</sub>), where U is the scalar wavefield (for upgoing or downgoing waves), and the subscript i stands for x, y, or z. The k<sub>z</sub> component may be computed via the dispersion relation as a function of k<sub>x</sub>, k<sub>y</sub>, and ω.

After the downward continuation step, we Fourier transform the Poynting fields back to the (x,y,ω) domain. The P<sub>i</sub>(k<sub>x</sub>, k<sub>y</sub>, k<sub>z</sub>) fields will contain information about the propagation direction of the waves reaching the (x, y) location. For the source wavefield, that will typically be a single wave (the

first arrival), since the source is downward continued only and reflections are not propagated; however, the receiver wave will contain many arrivals. To select the propagation vectors for the arrival corresponding to the imaging time, we cross-correlate the receiver wavefield with the source wavefield, and normalize by the image:

$$P_i(x, y) = \frac{\int S(x, y, \omega) P_i(x, y, \omega) d\omega}{\int S(x, y, \omega) U(x, y, \omega) d\omega} \quad (2)$$

We further normalize the resulting vectors to obtain the local unit propagation vector computed at the time when the source signal reaches the (x,y) location.

Unit propagation vectors are computed in this fashion for both the source and receiver wavefields in shot record migration; let us call these vectors **u<sub>s</sub>** and **u<sub>r</sub>**, respectively. In our convention, they have z-components of opposite sign and are defined at every (x,y) position at the current depth. The incidence angle φ, dip angle α, and azimuth angle β of a reflection are related to **u<sub>s</sub>** and **u<sub>r</sub>** as follows:

$$\tan \phi = |\mathbf{u}_s - \mathbf{u}_r| \div |\mathbf{u}_s + \mathbf{u}_r| \quad (3)$$

$$\tan \alpha = |u_{s,z} - u_{r,z}| \div [|u_{s,x} - u_{r,x}| + |u_{s,y} - u_{r,y}|] \quad (4)$$

$$\tan \beta = |u_{s,y} - u_{r,y}| \div |u_{s,x} - u_{r,x}| \quad (5)$$

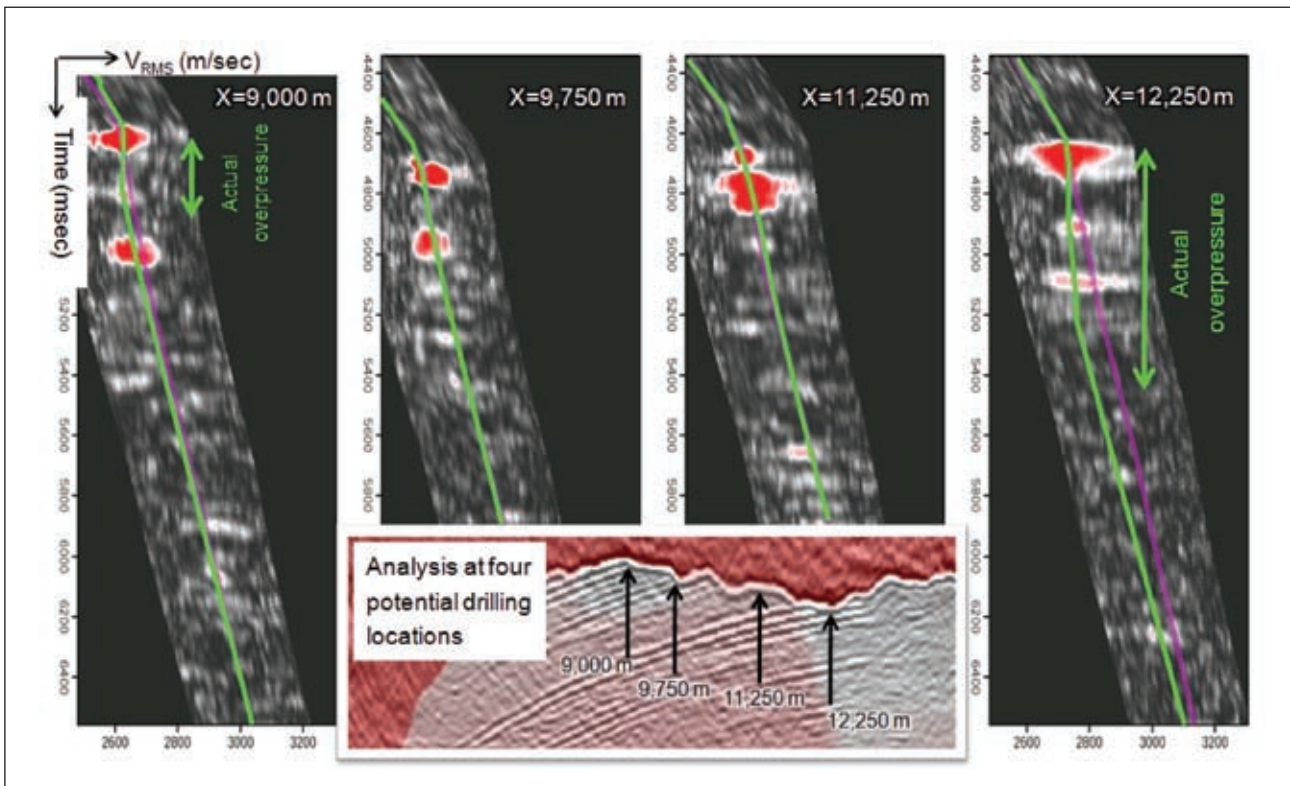


Figure 2 MVFA was applied at four potential drilling locations on the BP velocity benchmark model. The pink curves represent the migration velocity at the four locations. The green curves represent the true velocity. The red energy clouds are the velocity indicated by MVFA analysis.

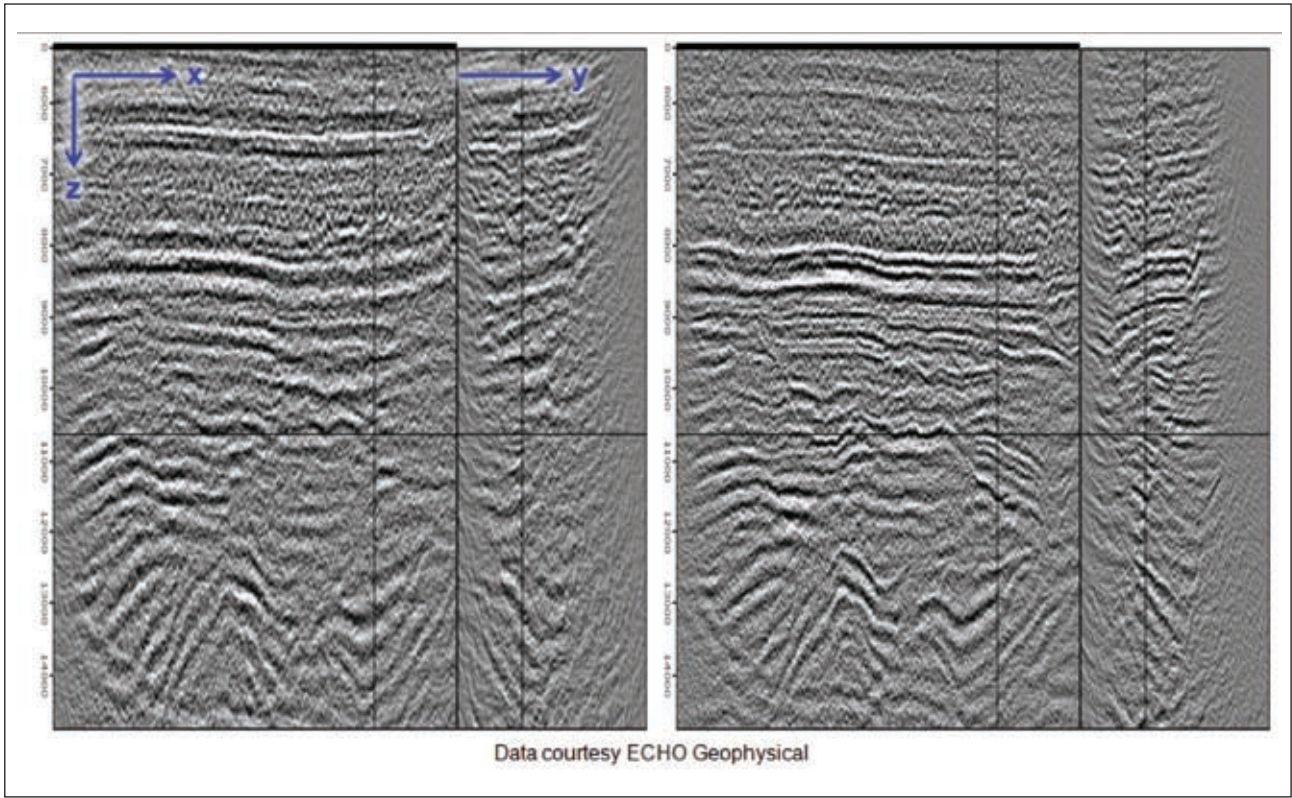


Figure 3 Left panel: WEM image of onshore South Texas data, using contractor stacking velocities converted to interval velocity in depth. Right panel: WEM image using migration velocity obtained by applying 8 iterations of MVFA, starting with a single  $v(z)$  function.

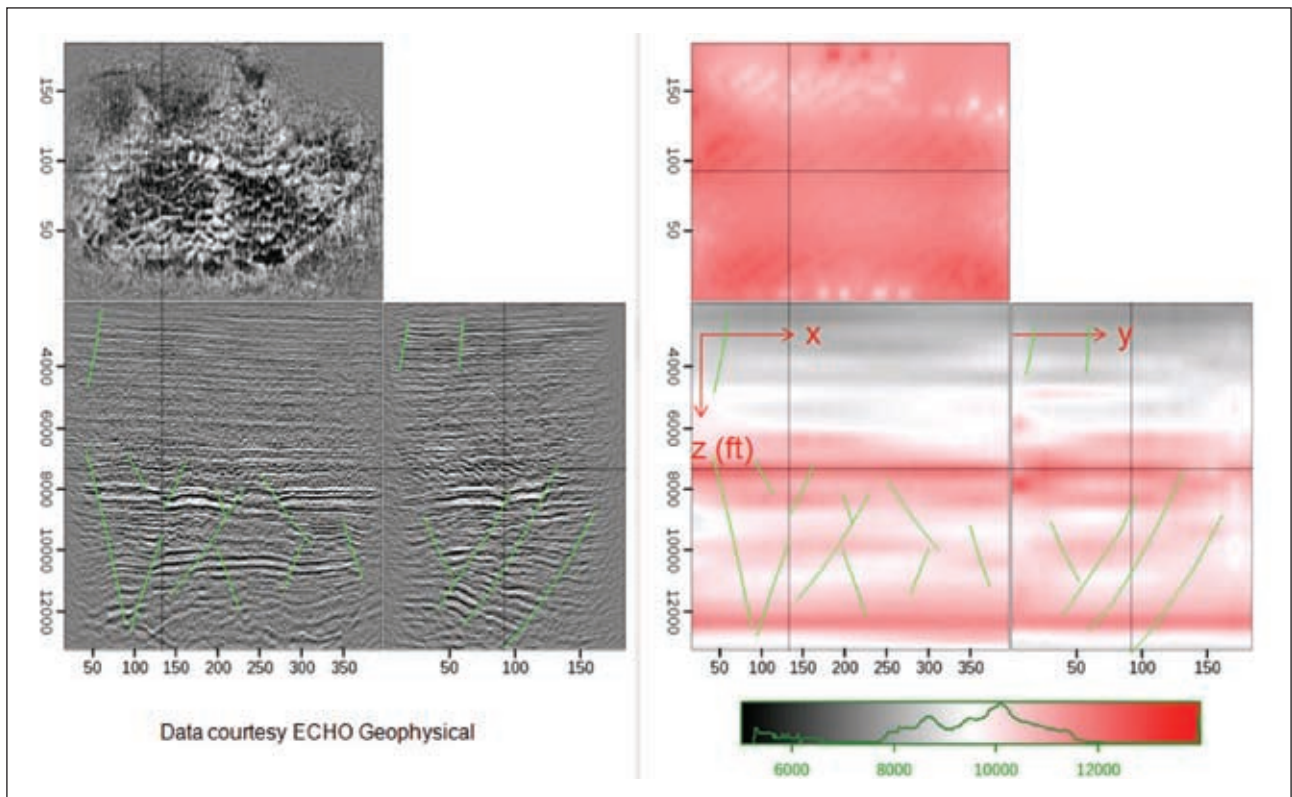


Figure 4 Left panel: image of South Texas, USA onshore example with MVFA-updated velocity. Right panel: velocity obtained after eight iterations of MVFA. Interpreted faults are shown on both panels.

The user defines a set of angle bins. The bins span a range of incidence angles, azimuth angles, and/or dip angles. For each (x,y) position at the current depth we calculate an  $u_s$  and  $u_r$ , and thus calculate the three propagation angles via equations (3), (4), and (5). When the source and receiver wavefields are correlated, the resulting image sample is placed into the appropriate bin.

**Examples**

Our first example utilizes the BP velocity benchmark model data and was adapted from Brown and Higginbotham (2009). The true velocity in this model has several anomalously low zones of P-wave velocity under the salt, corresponding to likely zones of overpressure, as is commonly found in the Gulf of Mexico. Unexpectedly high pore pressures just below the salt base present a serious drilling hazard, and cause many wells to be killed before reaching target depth. While P-wave velocity is not as sensitive as Poisson’s ratio to over-pressure, it is a readily available attribute for exploration wells.

MVFA is well suited to resolve velocity anomalies under salt because it uses WEM. Also, because it uses wavefield focusing rather than incidence angle to measure velocity error, it may be more robust to the limited incidence angle coverage typical of the Gulf of Mexico subsalt. In this example, we assumed that we knew the velocity perfectly down to the base of salt, but inserted a single  $v(z)$  function below the salt as a starting point for subsalt velocity analysis. Figure 2 illustrates the result of applying MVFA at four potential drilling locations under the salt, two of which are over overpressure anomalies. The challenge here is to see whether MVFA can resolve below-trend velocity deviations just under the salt. On the MVFA gathers at  $x = 9000$  m and  $x = 12,250$  m, there are overpressure anomalies, and the MVFA energy peaks do indeed indicate a subsalt slowdown, even though we migrated with too high a velocity. On the other two MVFA gathers, the energy peaks also line up with the true velocity, but are indicating that the velocity model is correct (an important check).

Our second example shows the performance of MVFA on an onshore dataset from South Texas, USA. The data are under-sampled in terms of source and receiver coverage, which hampers shallow imaging and degrades signal-to-noise ratio. Below the Wilcox Formation at about 7000 ft depth, the geology is more tectonically disturbed, with complex faulting. Overpressure is known to exist in this zone across the entire Gulf Coast, and when faults are able to seal, velocity contrasts appear across the faults, giving rise to the well-known fault shadow problem.

Application of a high-effort velocity inversion is critical to obtain an accurate image of fault shadow data like these. Figure 3 compares the result of applying WEM to the South Texas data with the contractor stacking velocity converted to interval velocity in depth with the velocity updated by eight iterations of MVFA. MVFA was applied at every shot point (972 over an area of ~80 km<sup>2</sup>) in the survey.

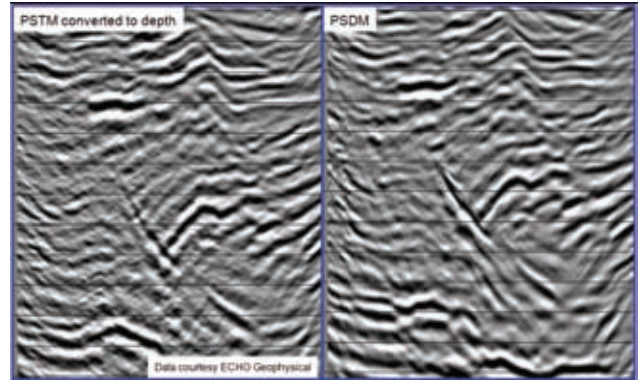


Figure 5 Left panel: PreSTM image of South Texas data. Right panel: WEM image with velocity model obtained by eight iterations of MVFA.

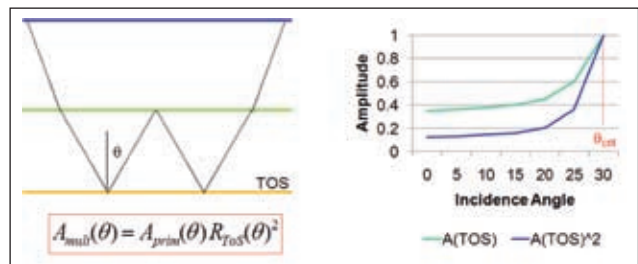


Figure 6 Left panel: schematic of a strong internal multiple which bounces twice off the top of salt (TOS). The amplitude-versus-angle (AVA) signature of the multiple is scaled by the squared AVA signature of the TOS. Right panel: the squared AVA signature of the TOS is over ten times stronger at the critical angle than at normal incidence.

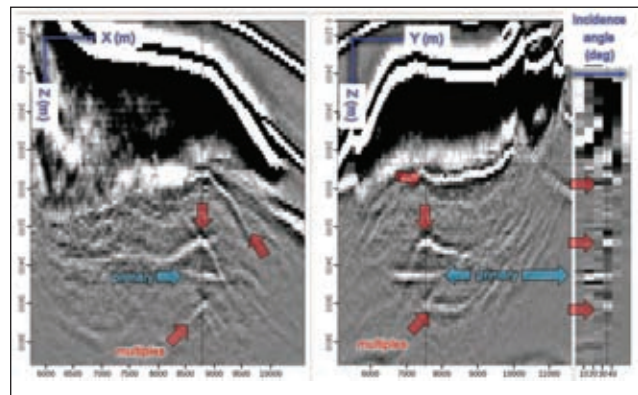
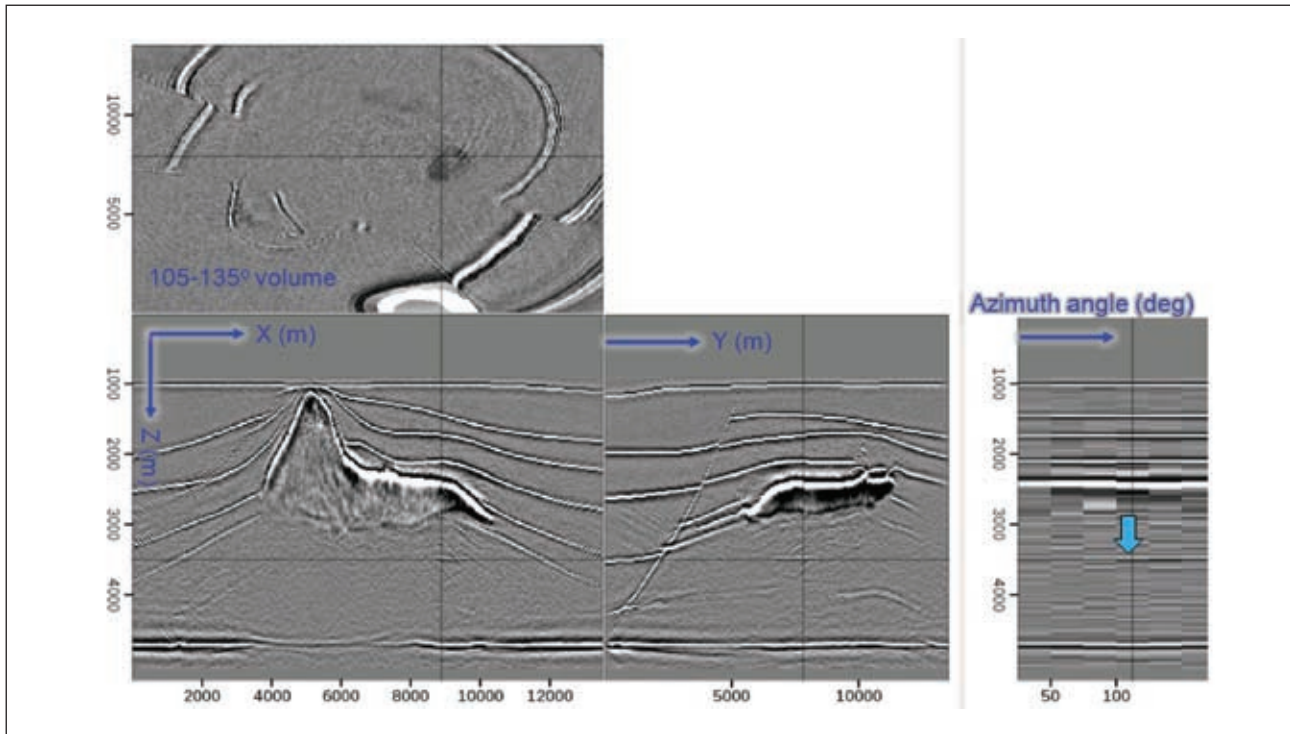


Figure 7 Left panel: zoom of (x,z)-plane of 30° common angle section from deepwater SEGIEAGE image, showing a single primary (blue arrow) and many strong internal multiples (red arrows). Centre panel: zoom of (y,z)-plane. Right panel: incidence angle gather illustrating critical angle spikes for train of internal multiples, with a more predictable AVA signature for the primary.

Exceptional improvements are seen in the imaging of fault truncations, with a general improvement in event resolution. It is important to notice that many areas on the left panel of Figure 3 are ‘dead zones’, with little obvious reflection energy, while the same portions of the image on the right panel contain numerous well-imaged events. This gets to the core of MVFA’s robustness in difficult areas with incomplete illumination. The sparse acquisition geometry in this example leads to poorly sampled angle gathers and a lot of noise. When the velocity is incorrect, angle gathers may not contain



**Figure 8** Left panel: 3D exploded slice view of the SEG/EAGE WEM azimuth image. The 105–135° angle volume is shown. Crosshairs are centred on sub-salt sand. Right panel: azimuth angle gather at  $(x,y)$  location of sub-salt sand.

any recognizable signal, much less a pristine event obviously curving up or down.

Figure 4 compares the final South Texas WEM image with the final velocity model, obtained after performing eight iterations of MVFA with an automatic velocity interpretation technique to rapidly pick focusing maxima. The depth slice of the 3D data viewer cuts through the Wilcox formation, and the image depth slice shows extensive local faulting. MVFA has successfully picked up the high seismic velocity inside the Wilcox layer, as well as the velocity inversion below the chalk. Looking closely across faults, notice how MVFA has measured some fairly significant velocity variations. Measuring these variations is the key to solving the fault shadow problem.

Figure 5 compares prestack time migration (PreSTM) to the final WEM image of the South Texas data. Notice in both cases a large regional fault with strong fault plane reflection. Velocity variations to the left of this fault cause a large sag in depth on the left side of the PreSTM image. On the PreSDM image, the deep strong reflection is much flatter, with interpretable faults along its length.

Figures 6–8 highlight our 3D angle decomposition technology for WEM. We simulated an acoustic, deepwater adaptation of the SEG/EAGE salt model. 1764 full-azimuth split-spread shot records were simulated over the model, with a shot spacing of 320 m and maximum offset of 4320 m in  $x$  and  $y$ . Free surface multiples were not modelled.

Figure 6 illustrates a strong internal multiple from the top of salt which provides an excellent test of our incidence

angle decomposition. The angle-dependent amplitude (AVA) of this particular multiple will resemble the reflection off the multiple generator (above the top of salt), but will be scaled by the squared AVA of the top of salt reflection. Since the top of the salt reflection is largest at critical angle (about 30°), the internal multiple's AVA signature will resemble a spike at the critical angle.

Figure 7 shows an exploded view of a 4D volume consisting of a set of fully-sampled incidence angle volumes, and zoomed to show a subsalt region affected by internal multiples. The data were migrated with the true velocity. The blue arrow illustrates the lone primary in the area, a flat sand layer, which has a maximum incidence angle of about 25°, due to salt refraction. Red arrows illustrate internal multiples. The left and centre panels show the 30° incidence angle volume, while the right panel shows an angle gather centred on the subsalt sand event. This example is especially interesting because the internal multiples effectively represent angle impulse responses. Our angle decomposition has positioned the events correctly near 30°.

Figure 8 similarly illustrates a 4D volume, but rather than incidence angle, shows an azimuth angle volume, consisting of six azimuth images with an azimuth bin width of 15°. The data were migrated with the true velocity. The left panel shows the 105–135° azimuth volume. Again, the crosshairs are centred on the subsalt sand. The right panel illustrates an azimuth angle gather located at the  $(x,y)$  position of the sand. The shot records used to form the image had full-azimuth coverage, so it is not surprising

that the shallow events show little variation with azimuth. However, under the salt, the sand event has a significant azimuth preference. This result highlights the significant illumination effects that salt can cause when refraction is an issue.

### Conclusions

In this article, we presented an approach to velocity model building in complex media, MVFA, which uses time-shift gathers from wave equation PreSDM and converts migration time shifts to perturbations in RMS velocity. We also presented a new technology to compute 3D angle information from WEM. We showed that MVFA can measure velocity deviations under salt, in the BP velocity benchmark example, with the potential to highlight subsalt overpressure anomalies. On a South Texas, USA onshore example, we showed how MVFA overcame limited acquisition effort and noise to accurately measure a complex velocity field, leading to improved imaging under fault shadows. Finally, we used a deepwater variant of the SEG/EAGE salt model data to highlight our angle decomposition technology. The successful angle imaging of a salt-related internal multiple demonstrates that our technique is accurate, both in terms of kinematics and amplitudes. The use of azimuth angle gathers enables detailed understanding of difficult illumination problems, such as those seen under Gulf of Mexico salt.

### Acknowledgements

We thank Bob Clapp of Stanford University for many useful conversations, and for his development of the multi-dimensional slice viewer used here. We also thank ECHO Geophysical and BP for allowing us to show the data examples shown herein.

### References

- Audebert, F. and Diet, J.P. [1993] Migrated focus panels: focusing analysis reconciled with prestack depth migration. *63<sup>rd</sup> SEG Annual Meeting*, Expanded Abstracts, 12, 961-964.
- Biondo, B. and Symes, W.W. [2004] Angle-domain common-image gathers for migration velocity analysis by wavefield-continuation imaging. *Geophysics*, 69, 1283-1298.
- Brown, M.P. and Higginbotham, J.H. [2009] Sub-salt overpressure detection before drilling using wave equation migration technologies. *79<sup>th</sup> SEG Annual Meeting*, Expanded Abstracts, 28, 1800-1803.
- Claerbout, J.F. [1985] *Imaging the Earth's Interior*. Blackwell, Oxford.
- Clapp, R.G. [2001] *Geologically Constrained Migration Velocity Analysis*. PhD thesis, Stanford University.
- Faye, J.P. and Jeannot, J.P. [1986] Prestack migration velocities from focusing depth analysis. *56<sup>th</sup> SEG Annual Meeting*, Expanded Abstracts, 5, 438-440.
- Fliedner, M.M. and Bevc, D. [2008] Automated velocity model building with wavepath tomography. *Geophysics*, 73, VE195-VE204.
- Gazdag, J. and Squazzero, P. [1984] Migration of seismic data by phase shift plus interpolation. *Geophysics*, 49, 124-131.
- Higginbotham, J.H. [1993] Prestack turning ray imaging with a 60 degrees operator. *55<sup>th</sup> EAGE Conference & Exhibition*, Extended Abstracts, C018.
- Higginbotham, J.H., Brown, M.P., and Clapp, R.G. [2008] Wave equation migration velocity focusing analysis. *78<sup>th</sup> SEG Annual Meeting*, Expanded Abstracts, 27, 3083-3087.
- Higginbotham, J.H. and Brown, M.P. [2009] Wave equation simulation and angle-domain imaging for acquisition testing, velocity analysis, and more. *71<sup>st</sup> EAGE Conference & Exhibition*, Extended Abstracts, U040.
- MacKay, S. and Abma, R. [1992] Imaging and velocity estimation with depth-focusing analysis. *Geophysics*, 57, 1608-1622.
- Prucha, M., Biondi, B. and Symes, W. [1999] Angle-domain common-image gathers by wave-equation migration. *69<sup>th</sup> SEG Annual Meeting*, Expanded Abstracts, 18, 824-827.
- Rickett, J. and Sava, P.C. [2002] Offset and angle-domain common image-point gathers for shot-profile migration. *Geophysics*, 67, 883-889.
- Sava, P.C. [2004] *Migration and Velocity Analysis by Wavefield Extrapolation*. PhD thesis, Stanford University.
- Sava, P. and Fomel, S. [2003] Angle-domain common-image gathers by wavefield continuation methods. *Geophysics*, 68, 1065-1074.
- Sava, P. and Fomel, S. [2006] Time-shift imaging condition in seismic migration. *Geophysics*, 71, S209-S217.
- Shen, P., Symes, W.W. and Stolk, C.C. [2003] Differential semblance velocity analysis by wave-equation migration. *73<sup>rd</sup> SEG Annual Meeting*, Expanded Abstracts, 23, 2132-2135.
- Vigh, D. and Starr, E.W. [2008] 3D prestack plane-wave, full-waveform inversion. *Geophysics*, 73, VE135-VE144.
- Wang, B., Mason, C., Guo, M., Guan, H., Yoon, K. and Li, Z. [2008] Subsalt velocity update using RTM-based DT scan. *78<sup>th</sup> SEG Annual Meeting*, Expanded Abstracts, 27, 3265-3269.
- Yoon, K. and Marfurt, K. [2006] Reverse-time migration using the Poynting vector. *Exploration Geophysics*, 37, 102-107.

Received 6 November 2009; accepted 9 January 2010.